Bull Volcanol (2003) 65:165–181
DOI 10.1007/s00445-002-0251-0

RESEARCH ARTICLE

M. G. Petterson · S. J. Cronin · P. W. Taylor · D. Tolia · A. Papabatu · T. Toba · C. Qopoto

The eruptive history and volcanic hazards of Savo, Solomon Islands

Received: 16 August 2001 / Accepted: 11 September 2002 / Published online: 23 November 2002

Abstract Savo Island is the 6-km-diameter emergent summit of an andesitic-dacitic stratovolcano, rising from the Iron Bottom Sound, 35 km NW of Honiara, Solomon Islands. Savo has erupted at least three times within recorded history and the 3,000 inhabitants maintain extensive oral traditions of past events. Through description and interpretation of the volcaniclastic sequences on the island, in conjunction with historical accounts and oral traditions, we reconstruct the eruptive processes on Savo. Block-and-ash flow (BAF) deposits are volumetrically dominant on the island within three main depositional environments: near-vent sequences, thick medial channel sequences and distal fan sequences. The deposits comprise universally non-vesicular and highly porphyritic (40–70% phenocrysts), high-silica andesite and dacite clasts. These appear to have been derived from collapsing lava domes during an 1560–1570 A.D. eruption. However, eyewitness descriptions and crater morphology suggest that similar deposits formed from dome explosions or collapses of eruption columns during later eruptions (1830–1840 A.D.). The high-sodium magmas (ca. 5–7 wt% Na_2O) apparently crystallised and strongly degassed prior to eruption. Shallow explosions were possibly caused by entrapment of magmatic gases beneath a dome or conduit plug of highly crystalline, near solid magma. Repeated sealing of the vent may have been due to inward collapse of the highly altered rocks of the surrounding hydrothermal system; these rocks probably were saturated due to contemporaneous high intensity rainfall events. BAFs were hot enough to char vegetation and attain aligned clast TRM (thermal remnant magnetism) up to 3 km from the vent, many being accompanied by ash-cloud surges. Changes with distance in the BAF deposits appear mostly dependent on flow confinement and are limited to an overall decrease in thickness and maximum clast size, and an increased definition of weak planar fabrics. In distal fan sequences, there is strong evidence for syn- and post-eruptive redeposition of primary deposits. Since the Savo population is concentrated on coastal volcaniclastic fans, we consider the greatest volcanic risk to life is from BAFs, associated ash-cloud surges and lahars. Hence, the main channels and fans are designated as the highest of three relative hazard zones on a simple map prepared to aid local education and planning initiatives on Savo.

Keywords Block-and-ash flows · Lahars · Lava domes · Solomon Islands · Vulcanian explosions

Editorial responsibility: J. McPhie

M.G. Petterson
British Geological Survey, Keyworth, Nottingham, NG12 5GG, UK

S.J. Cronin (✉)
Institute of Natural Resources, Massey University, Private Bag 11 222 Palmeston North, New Zealand
e-mail: scronin@geomar.de
e-mail: s.j.cronin@massey.ac.nz
Tel.: +49-431-6002139
Fax: +49-431-6002924

P.W. Taylor
Australian Volcanological Investigations, P.O. Box 291, Pymble NSW 2073, Australia

D. Tolia · A. Papabatu · T. Toba · C. Qopoto
Ministry of Energy Water and Mineral Resources, Mines and Minerals Division, P.O. Box G37 Honiara, Solomon Islands

Present address:
S.J. Cronin, GEOMAR Forschungszentrum, Abt. Vulkanologie und Petrologie, Wischhofstrasse 1-3, 24148 Kiel, Germany

Introduction

Savo Island is the emergent upper 485 m of an andesitic to dacitic stratovolcano, rising 1,400 m from Iron Bottom Sound, 35 km NW of the Solomon Islands capital Honiara (Fig. 1). Up to 3,000 inhabitants coexist with the volcano, which has erupted explosively several times, as recorded in written and oral history. Inhabitants are dispersed among small villages and settlements along most of the coastal fringe of the island. Eruptive products from the

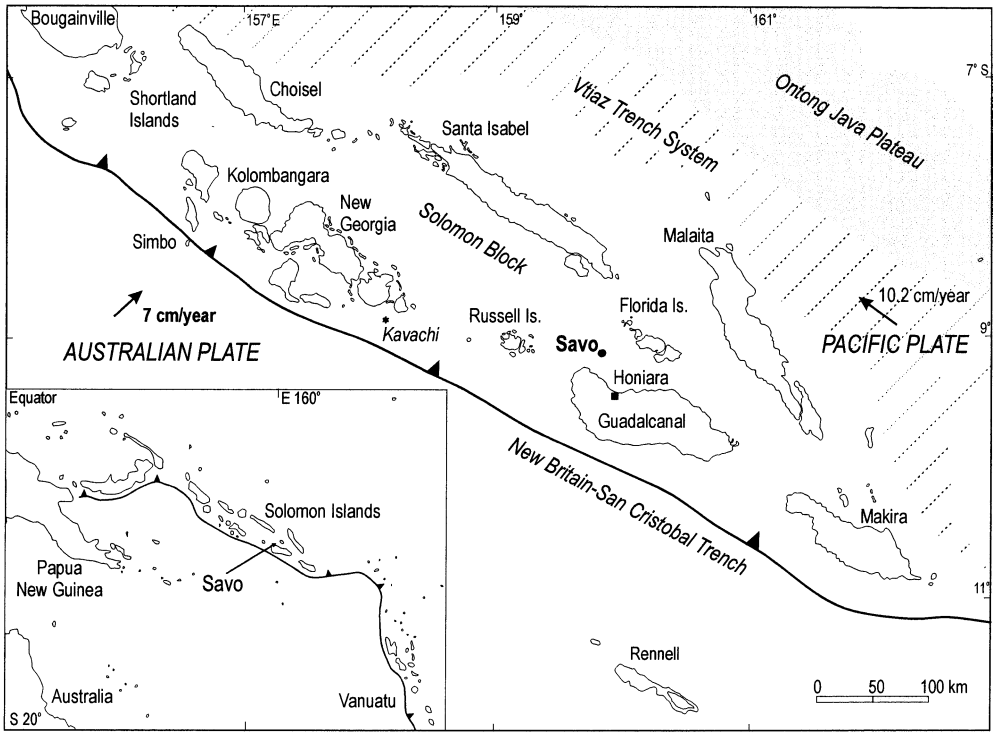

Fig. 1 Solomon Islands in relation to the Miocene Vitiaz Trench System (*hatched*) and the active New Hebrides-San Cristobal trench. Nearby major features include the Ontong Java plateau (with *crosses*), north of the Solomon block. Note the highly oblique convergence of the Pacific and Australian plates. Figure adapted from Petterson et al. (1999)

central vent are unusually well exposed (for a moist tropical environment) within several radiating drainages. Superficially, the characteristics of the deposits suggest Savo has parallels with several recently active, dome-forming volcanoes including Unzen, Redoubt and Montserrat, although the vertical relief of Savo is not quite as dramatic. Like these three other volcanoes (Gardner et al. 1994; Cole et al. 1998; Miyabuchi 1999), the exclusively non-vesicular clasts within the volcaniclastic deposits on Savo may be related to disruption of lava domes. However, present crater morphology, plus eyewitness accounts, suggest that external water within a shallow hydrothermal system and temporary crater lakes played an important role in recent Savo eruptions.

Through analysis of the sedimentary features and lithology of the deposits, coupled with eyewitness accounts and legends, we interpret eruptive processes at Savo. In addition, we outline the changes in deposit character with distance from source on this small volcanic island, and implications for downstream flow transformation within block-and-ash flows (BAFs). Using the interpreted volcanic history of Savo as a guide, we produce a simple volcanic hazard map for the island, to be used within local risk management initiatives.

Tectonic and geological setting

The Solomon Islands are part of the Greater Melanesian Arc, formed at the boundary of the Australian and Pacific Plates. Southward subduction of the Pacific Plate along the Vitiaz Trench System north of the Solomon Islands occurred up to 12 Ma (Yan and Kroenke 1993). Since that time, there has been northward subduction of the Australian Plate along the New Britain-San Cristobal Trench (Fig. 1), although there may have been further intermittent and local activity along the Vitiaz Trench System (Petterson et al. 1997, 1999). The Ontong Java Plateau collided with the Solomon Arc from ca. 12–9 Ma; uplifted portions of the plateau form some of the larger islands (Coleman 1966; Petterson et al. 1999). Other islands are a combination of ocean-floor and plateau lithologies, constructed during the two major arc-building periods (stage 1, Eocene–Lower Miocene; stage 2, Upper Miocene to present day). The present-day arc comprises the New Georgia Group, Russell Islands and Savo, together with many tens of submarine volcanoes south of the New Britain–San Cristobal Trench (Crook and Taylor 1994; Kroenke 1995).

Savo is a single stratovolcano constructed on unknown basement above ca. 14-km-thick crust (Furumoto et al. 1976), and represents the easternmost limit of the New Georgia terrain (Petterson et al. 1999). It is a modern, northern extension of the Mio-Pliocene to Recent Gallego Volcanic Field of NW Guadalcanal (Hackman 1980). A number of variably eroded centres in the Gallego field resemble Savo in size, geochemistry (Stanton 1994) and form, with andesitic–dacitic dome complexes and block-and-ash flow fans dominant.

Savo is a slightly elliptical 6×7-km-diameter island (Fig. 2), with a basal diameter of 9 km at 900–1,000 m below sea level and an estimated volume of 10 km^3. A 1.5×1-km crater (long axis oriented NE–SW) dominates

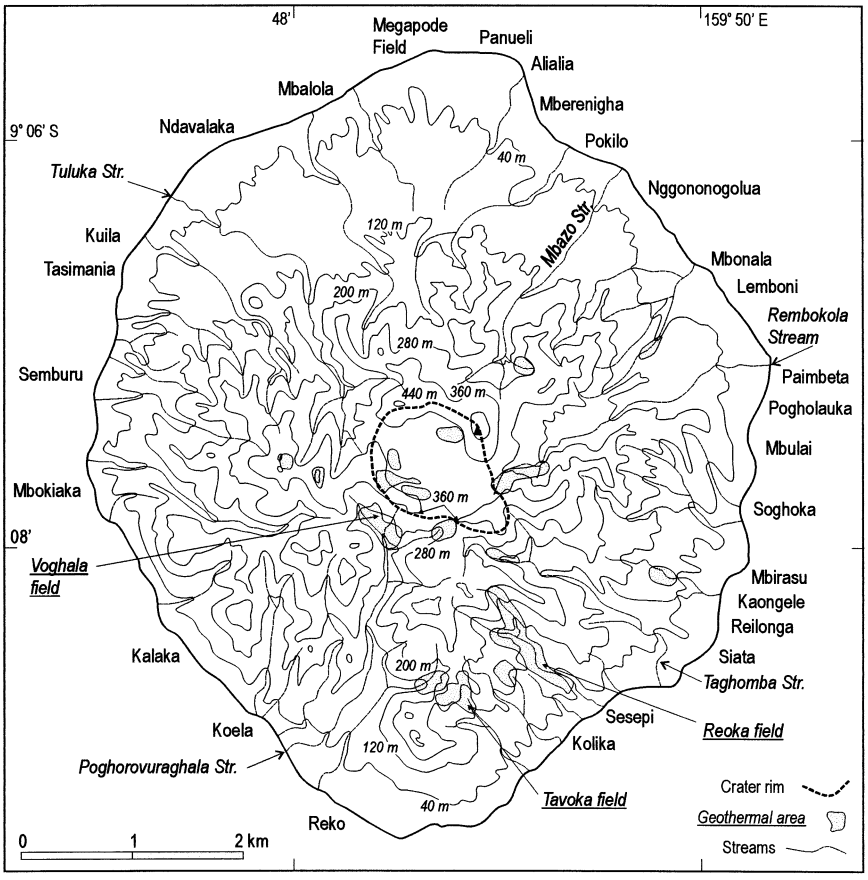

Fig. 2 Topography of Savo Island, showing the main stream channels, crater, coastal village names and the extent of presently active geothermal fields (*stippled*). Topographic contours shown at 40, 120 200, 280, 360 and 440 m elevation

the central summit area, the floor of which is mostly about 80 m lower than the lip (Fig. 2). A small, forested dome occupies part of the crater floor, whereas a second dome straddles the north-eastern crater rim and upper Mbazo valley (Fig. 3). Larger, older domes and exhumed cryptodomes, many of which reach 240 m high, are mostly located in the southern to south-western sector of the island. A drainage network radiates outward from the crater area, with well-developed coastal volcaniclastic fans formed at each one of the several channels. The steeply dipping medial flanks of the volcano are highly dissected, in places forming a series of radial steep-sided ridges and deep intervening valleys. Primary and secondary rain forest cloaks much of Savo. Unforested areas are related only to hydrothermal activity and, near the coast, agriculture.

A large number of hydrothermal areas are located on Savo and offshore, including features such as fumaroles, small geysers, hot-water springs and areas of steaming ground (Fig. 2). They are mainly concentrated around the central crater and south-eastern sector of the island (Toba 1995), although inhabitants in other sectors have reported additional newly formed areas, including offshore hot springs (Cronin et al. 2000b). Ad hoc monitoring of some of the hydrothermal fields over the last 40 years shows essentially constant temperatures, ranging mostly between 92 and 103 °C (Toba 1995). Temporal variations in temperature are not synchronous at separate fields, and are probably controlled more by local groundwater circulation than regional heat-flow changes. Hence, it appears that the near-surface environment has been in thermal equilibrium with underlying deep-seated magma for at least the last 40 years.

The unvegetated hydrothermal fields are mostly formed in highly altered volcaniclastic deposits. The area, depth and degree of alteration are high in near-crater, upper flank locations such as the upper Poghorovuraghala valley (Fig. 2), where frequent and large-scale collapses occur, generating locally destructive lahars, such as in 1998 (Cronin et al. 2000b).

Intermittent seismic recording on Savo has detected several tectonic earthquakes, including three events in 1985 located close to the eastern and south-eastern Savo coast and at <1 km focal depth. These may relate to a faulted south-eastern margin of the stratovolcano. During an in-crater field experiment in 1994 involving M. Lardy (ORSTOM, Vanuatu), M. Larue (SOPAC, Fiji), M. Petterson and T. Toba (Mines and Minerals Division, Solomon Islands), volcano-tectonic earthquakes were noted during 2 h of recording with a portable seismometer.

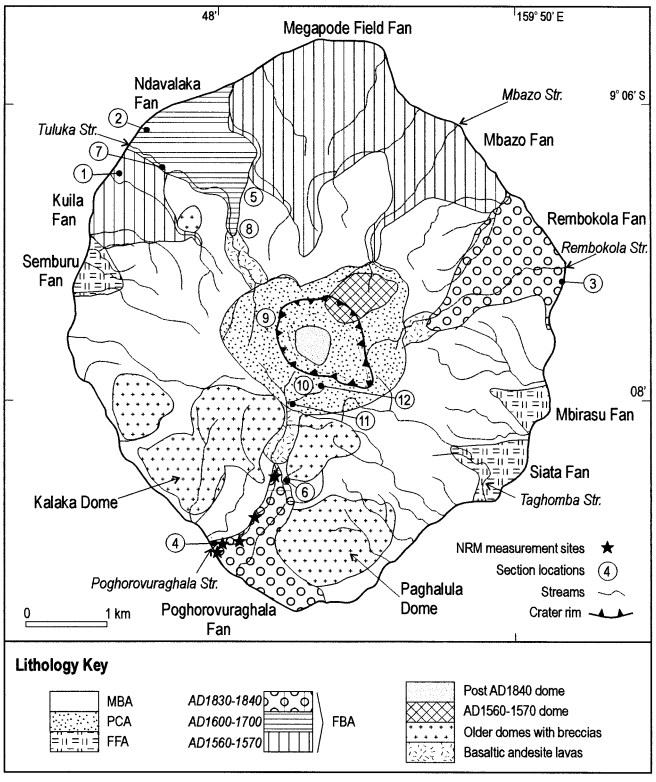

Fig. 3 Geological map of Savo, showing the four mapped volcaniclastic facies associations (Table 2) as well older domes and lavas. Locations of sections presented in Figs. 5, 7 and 9 are *numbered*, and *stars* denote locations of flux-gate magnetometer measurements

Historic eruption records

The first written record of a Savo eruption was made in the journal of Spanish mariner, Alvaro del Mendaña, who observed Savo erupting in 1568 (Guppy 1887; Amherst and Thomson 1901). The log records volcanic plumes, falling ash and the presence of white "roads" cutting through the jungle from the centre of the island to the northern shore (Amherst and Thomson 1901).

Guppy (1887) recorded a second protracted period of activity in the 1830s to mid 1840s, with intermittent (phreatic?) activity continuing until the 1880s. Local descriptions of the events included: "erupted materials rushed down deep channels", to form smooth surfaces that "look like roads from the sea"; "large quantities of water, dust and ash were ejected"; "day and night were the same"; "dust affected adjacent islands"; "several natives were killed". Guppy (1887) also noted that, up until 1877, volcaniclastic deposits were unvegetated, resembling roads, which afforded easy access to the summit.

Grover (1958) also provided an account of the 1830s–1840s eruptions, as related by Bishop J. M. Aubin, who, after arrival in 1906, noted local descriptions of the eruption. Mass evacuations took place during the height of eruptions – "stories are told of efforts to get away by canoes of which there were not sufficient for all: how women and children were clubbed in the struggle, and hands clinging in desperation to the gunwales were chopped off without mercy" (p. 107, Grover 1958). The eruption felled trees with a "glowing cloud" in the south-western sector, and fallen trees pointed seaward. Grover (unpublished record 1961; reproduced in Toba 1993) recorded an account of one of the climactic episodes of the 1830s–1840s eruptions from the perspective of a Guadalcanal inhabitant, related by the son of the eyewitness. The episode occurred before Europeans settled in the Solomon Islands, at a time of year around June/July and it was associated with heavy rain and earthquakes. It started in the afternoon in a small way, but by midnight there were sounds like the continued hooting of a steamer, and also like a river in flood rolling large boulders. Many repeated muffled explosions occurred, along with earthquakes at a rate of about 120 per minute. During the cataclysmic outburst that followed, the Guadalcanal Mountains and people standing outside their houses watching, were all lit up, as though by daylight. Millions of "great fiery rocks" were thrown into the sky above the fire on Savo, falling into the sea. A thin layer of ash covered the north-western coast of Guadalcanal. The explosions continued through the night and next day before dying out on the following night. Many Savo refugees arrived on Gaudalcanal by morning, and stayed for up to 10 years because the populated southern sectors of Savo had been rendered completely desolate (Fig. 4B).

Oral traditions, or kastom stories, as they are known in the Solomon Islands, are the main method of historical recording by Melanesian and Polynesian people (Bascom 1965). In many South Pacific locations, momentous or frightening events, such as volcanic eruptions are well recorded by oral traditions (e.g. Papua New Guinea, Blong 1982; Tonga, Taylor 1995; and Fiji, Cronin and Neall 2000).

Toba (1993) documented oral traditions on Savo through a series of villager interviews. Legends were consistent around the island, and all described local perspectives of two main eruptions.

An early event, termed by local inhabitants as the toghavitu eruption (meaning 7000 or 1007), was preceded by the filling of the crater with water, and then a period of increasingly violent earthquakes and tsunamis. The height of the eruption was marked by thunder, lightning, high seas and gale-force winds. All versions of the legend insist that no one was left alive on the island afterward. Processes described included fall of large blocks all over the island, and red-hot gaseous material flowing down valleys, "emitting foam". Later, mud and debris flowed down valleys like water into the sea. This process apparently built up the island to be much larger than its pre-eruption dimensions (Fig. 4A). Many people were killed by falling debris, being engulfed by both hot and cold flows and sinking into deposits. The "7000" or "1007" figure, depending on translation, represents the death toll. Almost the entire island was affected (Fig. 4A), leaving only a dusty grey remnant. Only a few survived by escaping to neighbouring islands, especially Guadal-

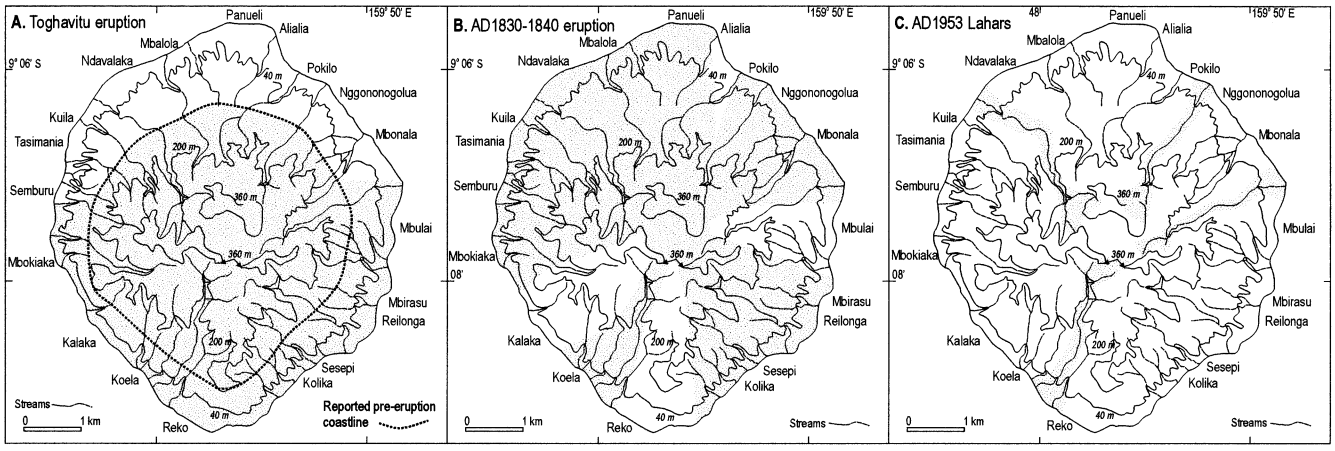

Fig. 4 Areas (*stippled*) affected by eruptions as described in Kastom legends from Savo as collected by Toba (1993). **A** Toghavitu event; *unstippled area* in the north represents the apparent "growth" of the island during this eruption. **B** 1830–1840 A.D. event. **C** 1953 A.D. lahar inundation

canal. Resettlement of Savo was apparently by Savo people who returned from Guadalcanal.

The second, later event, was preceded by similar signs as the toghavitu eruption, including filling of the crater with water, but it was smaller and some sectors in the south-west and east were not affected (Fig. 4B). Fewer people were killed (tens to hundreds) and many evacuated to safer places on Savo and to neighbouring islands, including Guadalcanal. These accounts correspond specifically to the 1830s–1840s eruptions described by Guppy (1887) and Grover (1958). Apparently a long period had elapsed since the toghavitu eruption, although the memories of that event were still strong, reinforced perhaps by the reputed occurrence of several other smaller eruptions in the interim period. Processes described included ash falls, which spread as far as the north-western coast of Guadalcanal. Local hazards included explosions, hot gas clouds, and flows within the valleys. Two types of flow were distinguished: those that burned people (pyroclastic flow or surge), and those into which people sank and drowned (lahars). There were periods of total darkness over the island and eruptions continued over a long period, impacting on different areas at different times. An additional account of this second major period of eruptions (Grover 1958) recorded how a woman escaped death by sheltering in a cave on the lee side of one of the south-western sector domes.

A third oral tradition, related by some of the villagers (Toba 1993), describes mudflows that originated from the crater area, possibly following a period of heavy rain in 1953. These inundated the main river channels of the island (Fig. 4C).

Eruption ages and timing

Both written accounts and oral traditions point to there being two major eruptions, as well as several other less catastrophic events. The legends of the second event correspond well with the long period of activity in the 1830s–1840s recorded by Guppy (1887) and Grover (1958). Despite there being no specific age ascribed to the earlier toghavitu event, it was reportedly a long time (several generations) before the second eruption and a long time before the settlement of Europeans. The event may relate to activity observed by Mendaña in 1568. However, Mendaña, also described there being many inhabitants on the island and bountiful gardens there (Amherst and Thomson 1901). These factors suggest that he arrived either some time before or after the catastrophic phase of activity as described in the toghavitu event.

A radiocarbon date of 270±45 years B.P. (NOAA15325, Dr G.S. Burr, University of Arizona, AMS facility) was obtained on a wood sample below 6 m of volcaniclastic deposits in the Ndavalaka fan of NW Savo (Fig. 3). The volcaniclastic deposits appear to reflect a single eruptive sequence, with no palaeosols or other evidence of long-term quiescence observed. The Oxcal 3.5 calibration program (Bronk-Ramsay 2002) and the calibration curve of Stuiver et al. (1998), indicate ages of 1520–1560 A.D. (P=0.42) and 1630–1670 A.D. (P=0.58) within 1σ error, and 1480–1680 A.D. (P=0.90), 1770–1810 A.D. (P=0.09) and 1930–1950 A.D. (P=0.01) within 2σ error. The most probable intercept predicted by Oxcal 3.5 and the CALIB4.3 program is 1645 A.D. If the most probable age-range of 1630–1670 A.D. is correct, the wood was contained either in the deposits of the 1830s–1840s eruption and had a ca. 200-year in-built age (i.e. age of the tree), or it was in the deposits from an earlier eruption, but subsequent to the pre-1568 event. Unfortunately, no further datable samples were collected during the initial stages of survey (1992–1995). Samples collected in 1999 from the uppermost units in the Poghorovuraghala fan were formed by the 1953 lahars and the 1830s–1840s activity and are too young for the ^{14}C method.

Table 1 XRF analyses of samples from selected map units on Savo

Sample	Ndavalaka fan[a]		Poghorovuraghala fan[a]				Rembokola fan[a]		Flank cryptodomes[b]		
	SV7B	SV7A	SV12	SV15	SV21	SV9	SV2	SV6B	SV27	SV28	SVI8
Loc.[c]	884929	884929	880882	886896	888902	880882	922918	922918	873894	873894	895885
Desc.[d]	bas and	hb and	hb and	hb-bi dac	hb dac	hb dac	hb dac	hb dac	basalt	Gabbro	Basalt
SiO_2	52.08	61.75	62.78	63.48	65.89	66.31	65.40	66.11	42.69	47.19	50.20
Al_2O_3	17.61	18.54	18.49	17.76	17.59	18.10	18.13	18.10	12.75	16.45	16.32
TiO_2	0.76	0.44	0.37	0.38	0.30	0.25	0.24	0.27	1.56	0.82	0.74
Fe_2O_3	9.04	4.58	3.75	3.90	2.88	2.23	2.14	2.77	16.95	8.96	10.06
MnO	0.15	0.10	0.08	0.08	0.06	0.06	0.06	0.06	0.18	0.17	0.14
MgO	3.6	2.16	1.55	1.73	1.19	0.85	0.79	1.06	10.18	8.40	4.70
CaO	7.9	5.12	6.81	4.08	3.24	2.40	2.48	3.35	10.90	12.80	10.61
Na_2O	4.22	5.62	6.04	5.50	6.24	7.28	7.21	6.48	2.73	3.21	3.57
K_2O	1.42	1.73	2.20	1.90	2.08	2.16	2.15	2.09	0.55	0.53	1.44
P_2O_5	0.24	0.20	0.17	0.18	0.06	0.07	0.10	0.13	0.09	0.06	0.19
Total	97.60	100.30	99.80	99.10	99.60	100.20	98.80	100.40	98.60	98.60	98.00
Zr	127.8	82.0	103.1	113.0	110.4	93.0	108.0	112.1	50.2	39.0	71.6
Y	11.4	22.1	16.4	10.0	5.7	4.0	4.7	7.5	20.6	21.3	19.0
Nb	5.7	3.1	3.7	4.7	5.0	3.0	5.3	4.7	2.5	1.5	3.1
Cr	44.4	36.1	40.1	48.6	24.2	10.0	9.9	18.2	27.7	188.4	133.9
V	114.6	305.9	207.4	103	77.2	52.0	58.3	74.2	603.2	352.6	413.3
Rb	28.5	17.7	24.7	35.3	29.7	47.0	34.5	29.2	5.6	4.4	11.8
Sr	1,159.5	669.3	873.2	1,096.8	1,198.6	1,190.0	1,191.8	1,205.2	373.2	388.9	855.2
Ba	743	333.1	422.4	716.3	797.9	881.0	991.4	784.5	144.2	106.4	530.4
Ni	22.6	20.2	13.1	13.4	12.8	5.0	6.9	9.8	35.2	41.6	33.7
Cu	20.1	104.1	23.7	27.2	8.0	11.0	12	14.6	66.1	81.3	119.7
Zn	58.6	74.8	52.4	47.3	38.5	37.0	40.1	46.0	96.3	65.1	86.5
Ga	21.7	20.3	20.2	20.7	19.7	n.d.	21.5	22.1	15.8	18.0	17.9
Sc	4.4	21.2	12.6	6.0	2.3	n.d.	2.4	6.9	71.9	55.8	33.0
Co	9.1	24.1	12.7	7.7	3.8	8.0	3.6	4.6	75.3	35.8	30.6
Th						6.0					
U						<3.0					
Pb						13.0					
Ce	22.0	33.7	21.8	26.5	6.4		19.7	14.9	13.9	14.9	40.2
Nd	7.1	17.9	6.7	10.4	2.5		7.3	5.3	4.7	4.8	17.9
La	8.3	11.4	10.2	8.2	2.7		3.3	6.0	6.6	3	18.3

[a] Samples from Ndavalaka, Poghorovuraghala and Remobokola fans are clasts from Dm(m)/Dpw(m) facies
[b] SV27 and SV28 are from the Kalaka dome, and SV18 from the Paghalula dome (Fig. 3)
[c] Loc Location, grid references all preceded with WK, from Sheet 9/159/8 (1975) of the Solomon Islands map series X711 (DOS 456)
[d] Desc. Hand specimen description; *bas and* basaltic andesite; *hb and* hornblende andesite; *hb-bi and* hornblende–biotite andesite; *hb dac* hornblende dacite; *hb-bi dac* hornblende–biotite dacite

Table 2 Lithofacies descriptors used for volcaniclastic associations on Savo

Associations	Code	Lithofacies[a]	Transport processes
Block-and-ash flow fan association	FBA	Dm(m) >Dpw(m) >>Sp, Ppw(c), Sc/Mc >Pc(c), Cc(c)	Block-and-ash flows, debris flows, tephra falls, surges, fluvial
Medial block-and-ash flow association	MBA	Dm(m) >>Dpw(m) >Spw, Ppw(c) >Sc	Block-and-ash flows, debris flows, tephra falls, surges
Proximal crater and flank association	PCA	Sp, Spw, Ppw(c), Dm(m), Dpw(m) >Pc(m), Sc	Tephra falls, block-and-ash flows, surges
Fluvial fan association	FFA	Pc(c), Sc, Dpw(m)	Fluvial, debris flows

[a]*Xy(z)*: *X* dominant grain size, *y* sedimentary structures, *z* matrix or clast support, where applicable; *X: D* diamicton (here used to describe a poorly sorted unit with a sand matrix containing distinctly coarser pebbles, cobbles or boulders); *C* cobble (64–256 mm); *P* pebble (2–64 mm); *S* sand (0.063–2 mm); *M* mud (<0.063 mm); *y: m* massive; *pw* weak planar fabric; *p* planar bedded; *c* cross bedded; *(z): m* matrix-support; *c* clast-support

Further evidence comes from the relative degrees of dissection and drainage densities on the volcaniclastic fans that encircle Savo. Aerial photographic interpretation suggests that the Rembokola and Poghorovuraghala fans are the least dissected, the Ndavalaka fan (where the radiocarbon date comes from) is intermediate, and the Kuila, Mbazo and Megapode Field fans are significantly more dissected, with a much higher drainage density. Hence, the Poghorovuraghala and Rembokola fans could relate to the 1830s–1840s eruptions, the Ndavalaka fan to an eruption some time between 1630 and 1670 A.D., and the Kuila, Mbazo and Megapode Field fans to the earlier toghavitu event.

The cryptodomes exposed in the south-western sector of Savo (Fig. 3) are probably the oldest units, but are too young for the K–Ar dating method attempted, that is <100,000 years old (David Rex, Leeds University, personal communication).

Composition and petrography

The volcaniclastic products of recent eruptions on Savo are volumetrically dominated by andesitic to dacitic compositions. Typical clasts in the youngest volcaniclastic deposits, within the Poghorovuraghala and Rembokola fans, are all very similar and are the most silicic of all samples analysed from Savo (62–66 wt% SiO_2; Table 1). The clast compositions of the older Ndavalaka fan are possibly less evolved, or at least at the low-silica end of the range within the younger fans. The most basic rocks (43–50 wt% SiO_2) include hornblendite or pyroxenite accessory clasts in the recent volcaniclastic deposits, and basalt and gabbro within domes and exhumed cryptodomes on the lower island flanks (Table 1).

The most common phenocryst assemblage includes hornblende + plagioclase + alkali feldspar + magnetite ± pyroxene ± biotite, with accessory sphene, apatite and zircon. Hornblende is commonly rimmed by magnetite. Almost all samples have high phenocryst contents (40–70 vol%) and a mostly cryptocrystalline groundmass; microcrystalline groundmass textures also occur. Common gabbroic enclaves consist of hornblende + pyroxene + plagioclase + magnetite.

Lithofacies and lithofacies associations on Savo

The complex volcanic sequence exposed on Savo is simplified by its classification into four lithofacies associations (Table 2), denoted by their main constituent facies. These recent volcaniclastic deposits on Savo overlie an apparent basement of basaltic andesite lavas, domes, and gabbroic–dioritic shallow intrusions (Fig. 3).

Block-and-ash flow fan association (FBA)

Six discrete areas of FBA are present (Fig. 3), five in the northern half of Savo, and one in the south (Poghorovuraghala). Each of these represent a fan, with an associated shallow offshore portion that is most likely composed of submarine volcanic mass-flow and turbidite deposits. The low-lying FBA fans have resulted in a significant enlargement of the aerial extent of the island and are economically important, being prime agricultural and habitation sites. The gross morphology of these fans comprises an upper valley-confined section and lower broader coastal section. The coastal fans are flat to gently undulating with a gentle seaward dip. Coastal erosion has trimmed these fans into small cliffs (1–6 m high), which afford good transverse-fan exposure.

Most sections show little or no evidence for long hiatuses and they probably represent deposition from single eruptive episodes. However, dark brown and reddish brown palaeosols are found in some exposures, along with major cut-and-fill structures in others, indicating that these fans are composite structures formed from the deposits of a number of rapid-deposition periods, interrupted by significant periods of slow deposition, stability or erosion.

The FBA is characterised by extreme variability (Figs. 5 and 6), vertically in exposures up to 9 m thick, and laterally over tens to hundreds of metres in sections at various angles transverse to palaeoflow directions.

The most abundant lithofacies [Dm(m); Table 2] is a massive 'diamicton'; this term is here used to denote a very poorly sorted deposit with a sand matrix that either supports or fills interstices between clasts of pebble to boulder size (commonly <0.5 m diameter; Fig. 6a). Single

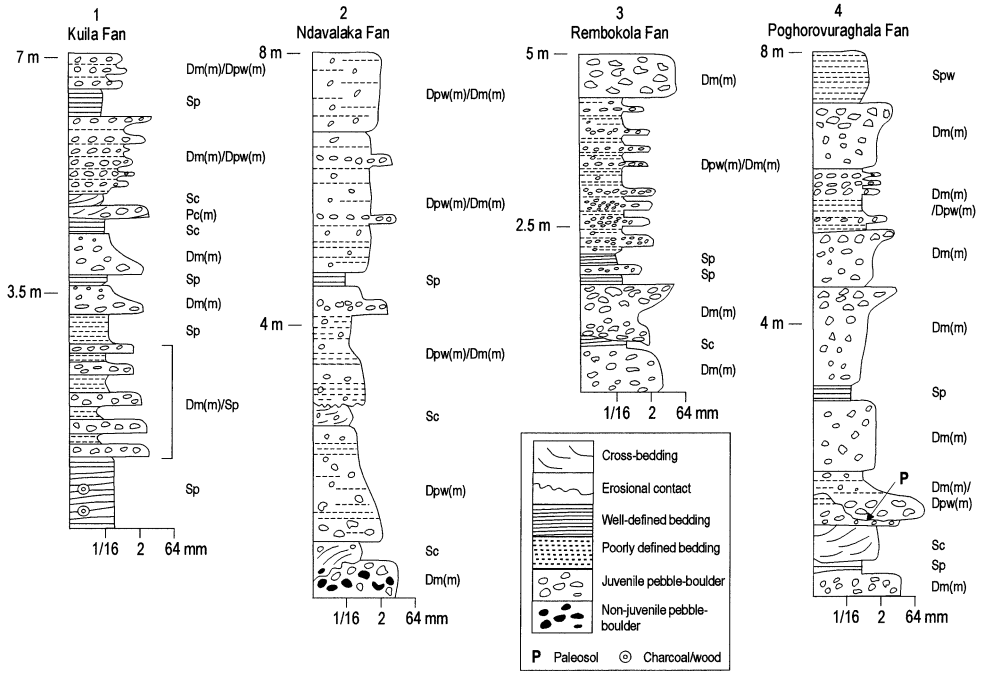

Fig. 5 Logged sections and facies interpretations within the FBA. Facies codes are given in Table 2. Numbered section locations are given on Fig. 3. Scale at column bases indicates modal grain size, estimated by point counting (50–100 clasts at each site), and field textural estimates for finer units

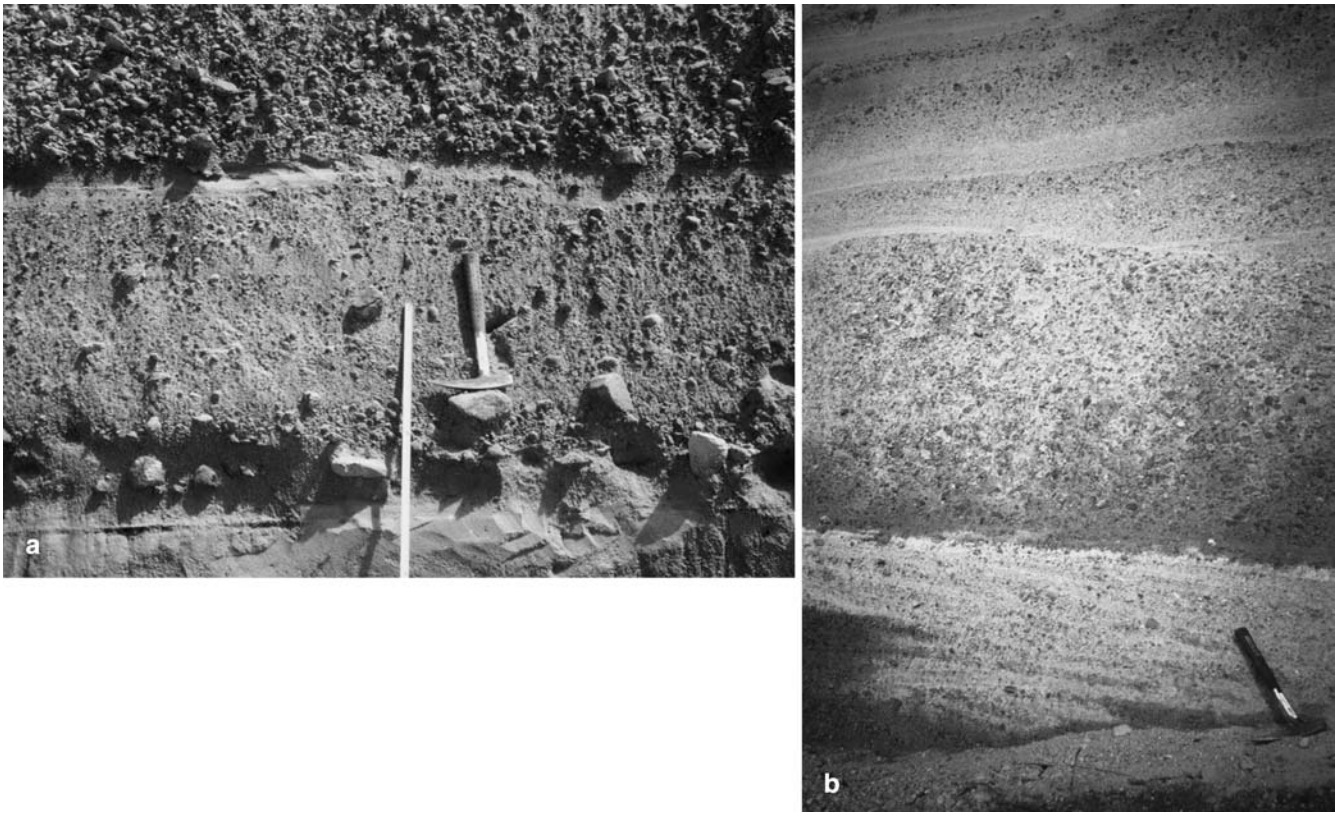

Fig. 6a,b Photographs of lithofacies in the FBA. **a** Typical Dm(m) unit in the Rembokola fan. Note thin Sp unit preserved at top, and underlying Sp that grades downward into Dm(m). **b** Stacked deposits exposed in the Ndavalaka fan, with coarse-tail reversely graded Dm(m) (and intercalated Sp) overlying massive Dm(m), which in turn overlies Sc and Pc(m)

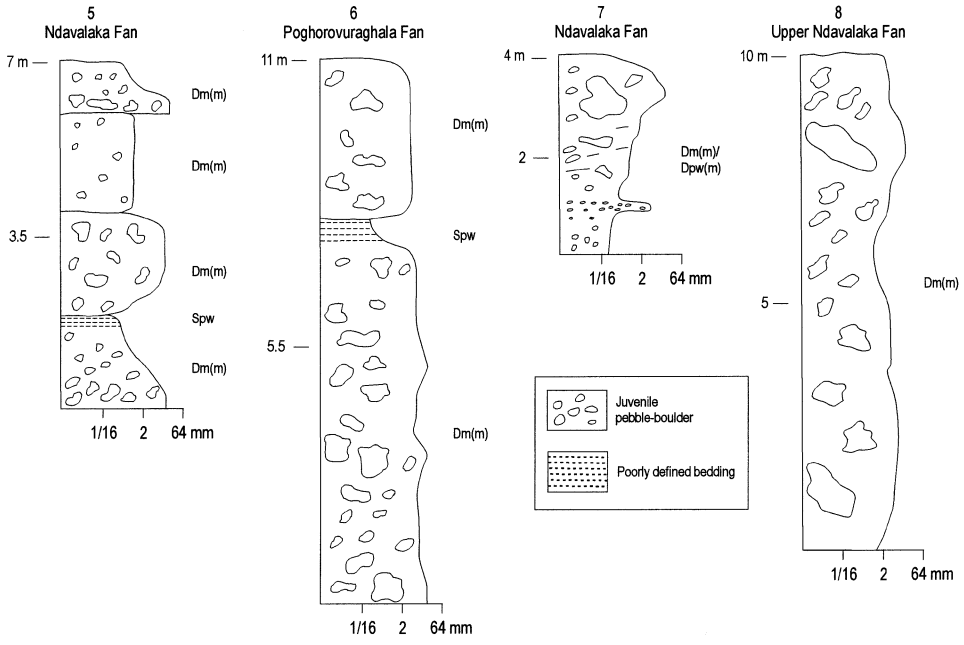

Fig. 7 Logged sections and facies interpretations from the MBA. Facies codes are given in Table 2. Numbered section locations are given on Fig. 3. Scale at column bases indicates modal grain size estimated by point counting (50–100 clasts at each site), and field textural estimates for finer units

depositional units range between 0.5 and >8 m thick. Clasts comprise 20–40 vol% of the deposits, increasing to >60% in clast-concentration zones and in coarser deposits. Clasts are uniformly non-vesicular, angular to subrounded, high-SiO_2 andesite to dacite, whereas the poorly sorted, fine-coarse sand matrix is pale brown to white, crystal and crystal-fragment rich; sand grains are highly angular. Subordinate clast lithologies include hornblende gabbro, basaltic andesite, gabbroic diorite, hornblendite and red and white hydrothermally altered clasts. The latter are conspicuous and make up 5–10% of the clasts, based on point counts made at most described sections. Deposit fabric, where present, comprises indistinct, horizontal, laterally discontinuous, matrix-poor, pebble- or cobble/boulder-concentration zones, sand layers, clast strings and alternating matrix- and clast-rich layers. Both normal and reverse coarse-tail grading occur. Charcoal fragments are common within some deposits.

At several sites within the Poghorovuraghala FBA (Fig. 3), in deposits correlated with the 1830s–1840s eruptions and the 1953 lahars, natural remnant magnetism (NRM) of 5–15 cm-diameter clasts was recorded using an FG Instruments BR-2 portable magnetometer (ten clasts measured at each site). This technique is a fairly reliable alternative to laboratory studies of remnant magnetism (Hoblitt and Kellog 1979). In the upper Poghorovuraghala valley, uniformly aligned NRM was found for clasts in Dm(m) units, which, in conjunction with the charcoal present, we interpret as thermal remnant magnetism, implying an emplacement temperature in excess of Curie Point (ca. 350 °C). In two further sites near the coast (Fig. 3), Dm(m) clasts had random NRM orientations.

Subordinate but still common lithofacies [Dpw(m), Fig. 5] are characterised by weak planar fabric, defined by discontinuous layers of sand or pebbles, and/or clast strings. NRM of coarse pebble- to cobble-sized clasts in two Dpw(m) units in the Poghorovuraghala catchment showed random NRM orientations.

Less common lithofacies, Sp and Ppw(c), consist of moderately well-sorted, horizontally bedded or laminated sand and pebble layers, 2–3 cm to 1 m thick. Some units contain charred or unaltered wood fragments and/or tree stumps in growth position.

Another minor lithofacies (Sc and Mc) comprises centimetre- to 1-m-thick, poorly sorted, fine sand-dominated beds containing pebbles and rare cobbles (Fig. 6b). These units are internally thinly bedded or laminated with low-angle cross-bedding in some locations (Fig. 5). Beds are distinguished by alternating fines-poor and fines-rich layers. Some units contain charcoal fragments.

Further lithofacies, Pc(c) and Cc(c), are commonly channel-filling, and are either cross bedded on moderate-high angles, or planar bedded, with alternating layers of medium–coarse sand, fine sand and pebble or cobble-rich deposits. Single beds are well sorted and the coarser deposits are clast-supported. Bed thickness ranges between centimetre- and metre-scale, and the coarsest deposits contain clasts up to 0.7 m diameter. Pc(c) and Cc(c) show the widest range of clast lithologies, commonly containing clasts of dacite, basalt and andesite as well as rare hydrothermally altered clasts.

Medial block-and-ash flow association (MBA)

Up to 50% of the area of Savo is mapped as MBA (Fig. 3), which probably makes up the greatest portion of the cone volume. Sections >40 m thick through these deposits are found within the mid-upper parts of the main river valleys (Figs. 7 and 8). Palaeosols are noted in some exposures, along with eroded contacts where coarse Dm(m) units are cut into weakly bedded Spw, Ppw(c) and Sc layers.

Fig. 8 The basal portion of a typical Dm(m) within the MBA, in the middle reaches of Poghorovuraghala catchment. Deposits of this uniform character dominate the mapped extent of the MBA. The *camera case* is ca. 25 cm high

Hence, these sections probably include deposits from several eruptive episodes separated by significant time breaks. Post-depositional hydrothermal alteration has cemented small portions of some deposits, with local development of fines-poor fossil fumarole vents.

The dominant lithofacies present is Dm(m) (Figs. 7 and 8), in beds 0.5 to >40 m thick, with most falling in the range of 2–10 m. The MBA is homogeneous in character, both vertically and laterally. The non-welded, very poorly sorted deposits contain clasts up to 2.5 m diameter (modal range of 0.3–0.7 m diameter based on point counting of 4–5 sections within each main catchment), supported within a matrix of fine sand to fine pebbly sand. Clasts are dominantly subangular-angular, and uniformly dense with no vesicular clasts found. Based on point counts of clast diameters and d-max measurements (the average of the maximum diameters measured from the five largest clasts observed in any given outcrop), a weak trend of decreasing maximum clast size with increasing distance from the crater is noted. Clast content varies between 10 and 60% by volume (modal range 20–40%). These units are dominated by andesitic to dacitic clasts (generally uniform in composition within any given stratigraphic unit), with 5–10% gabbro, basalt, basaltic andesite, hornblendite and hydrothermally altered clasts. Charcoal fragments are commonly found within Dm(m) units. NRM measurements on clasts at one location in the Poghorovuraghala Valley (Fig. 3) showed uniformly oriented magnetism.

The less common Dpw(m) lithofacies is similar to the MBA Dm(m), but contains weak fabrics defined by discontinuous, horizontal, sand- or pebble-rich layers or clast strings. NRM measurements on clasts at one location in the Poghorovuraghala Valley, where charcoal was also found (Fig. 3), showed uniformly oriented clast magnetism, whereas another showed random clast orientation.

Spw, Ppw(c) and Sc are minor lithofacies of MBA. These are pale brown, shower-bedded, laminated or low-angle cross-bedded units between a few centimetres and 1 m in thickness. Some of these units clearly cap Dm(m) units, whereas others may be related to the units directly above.

Proximal crater and flank association (PCA)

The PCA is distributed concentrically within 0.5–1 km of the summit crater, forming the steep inner and outer crater walls (Fig. 3). The upper tributaries of the major rivers originate on the lower slopes of the outer crater-wall

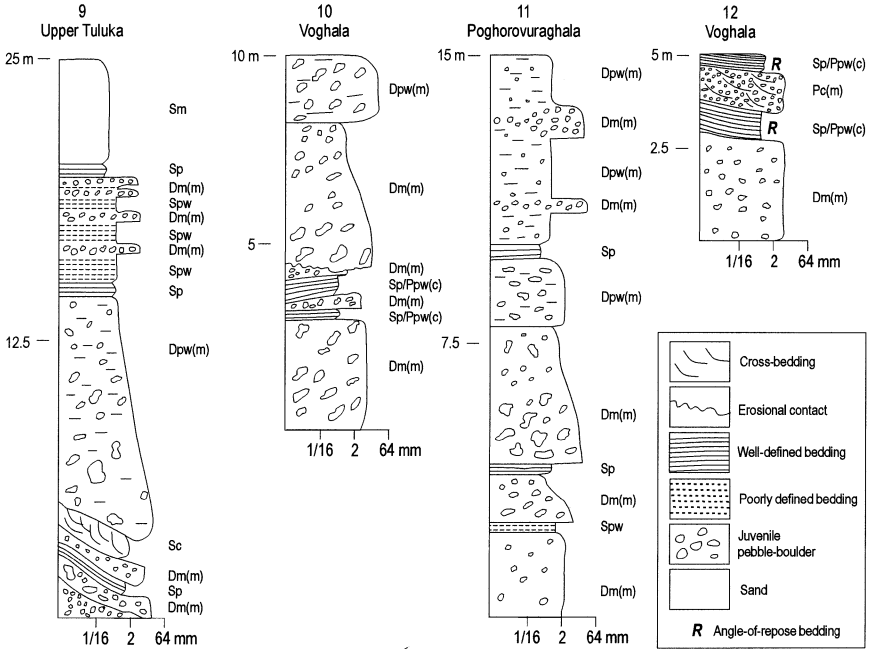

Fig. 9 Logged sections and facies interpretations from the PCA. Facies codes are given in Table 2. Numbered section locations are given on Fig. 3. Scale at column bases indicates modal grain size, estimated by point counting (50–100 clasts at each site), and field textural estimates for finer units. Note *scale for column 9* is different from that for the other three columns

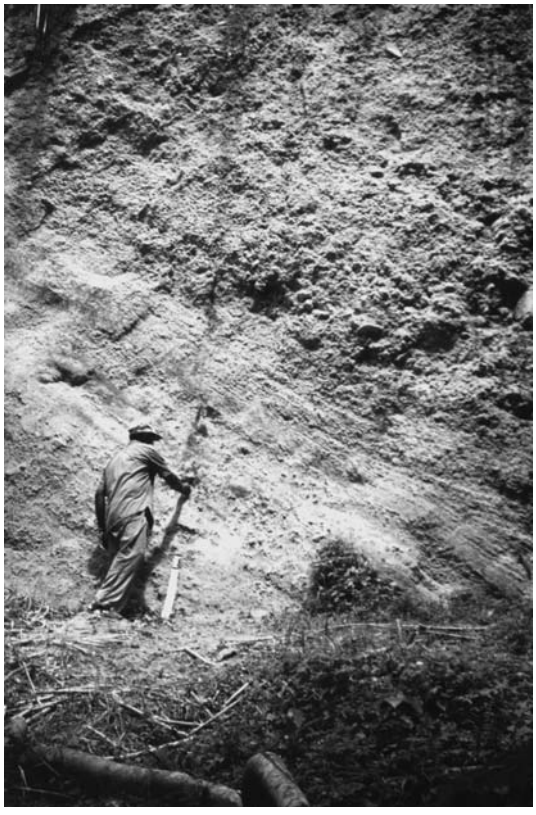

Fig. 10 PCA exposure in the present crater walls, including stacked Sp and Ppw(c) and intercalated Sc, overlain by massive Dm(m)

deposits. The crater rim ranges between 485 (island summit) and 280 m in altitude within a breach on the eastern side (Rembokola catchment), whereas the crater floor lies at ca. 220 m. Extensive hydrothermal alteration occurs in many parts of the mapped extent of PCA. The PCA is dominated by Sp/Spw, Ppw(c) and Dm(m)/Dpw(m) lithofacies, with lesser but important volumes of Pc(m) and Sc (Fig. 9).

The mantling and shower-bedded Sp, Spw and Ppw(c) (Fig. 10) are well sorted, commonly with alternating Sp and Ppw(c) beds in composite units up to 15 m in total thickness. The Ppw(c) ranges between 0.5 and 1 m in thickness, containing dense, subangular, andesitic clasts up to 6 cm in diameter. Sp ranges between 0.05 and 0.2 m thick, and contains rare outsized clasts up to 3 cm.

Dm(m) and Dpw(m) lithofacies are unwelded and maximum clast diameters are up to 0.6 m (modal range 7–15 cm diameter). Normal grading is common. Andesitic to dacitic clasts dominate, with ca. 10% subsidiary lithologies, as described for medial and distal Dm(m) units.

Sc and Pc(m) facies are intercalated with Sp and Ppw(c) units in beds <0.5 m in thickness, distinguished by their poorly sorted character, presence of outsized clasts and cross bedding. These beds are discontinuous and highly variable in thickness.

Fluvial fan association (FFA)

Three small triangular FFA areas occur along the lower reaches of minor and ephemeral stream systems (Fig. 3). They are sourced on the medial flanks rather than the crater area and have a limited inland extent. The representative Siata fan dips seaward more steeply than FBA areas and dominantly contains Pc(c) and Sc lithofacies. These units are moderately well sorted, thinly bedded (cm- to <m-scale), in both planar and cross beds, and contain clasts mostly <1 cm diameter. Clasts are dominantly andesite–dacite, although most other lithologies found on the island are also present as clasts, both unaltered and hydrothermally altered.

Minor volumes of Dpw(m) units are noted, and dominate a small number of outcrops. These beds contain coarse, angular clasts up to 0.3 m diameter, within fine–medium sand matrices. Clast lithologies are similar to the interbedded Pc(c) and Sc facies.

Domes and lava units

Crater domes

Two recent domes occur within the present crater area (Fig. 3). The smooth, central crater dome is ca. 500 m in diameter with a maximum height of ca. 30 m. Its summit is ca. 50 m lower than the lowermost portion of the crater rim. It is cloaked in dense forest except in areas with vigorous hydrothermal activity. Much of the surface rock is hydrothermally altered, but some areas preserve flow-fold structures, and fresh samples are silicic–andesite to dacite, medium to coarsely porphyritic, with hornblende and plagioclase phenocrysts dominant. Mafic and ultramafic, hornblende-dominated enclaves are present.

The second dome is 800×500 m in basal dimensions and located on the north-eastern crater margin within the upper Mbazo catchment. It comprises coarsely porphyritic pale-coloured silicic andesite to dacite, similar to the central crater dome. Based on geomorphic relationships and similarities in composition, this feature appears genetically related to the Mbazo and Megapode Field volcaniclastic fans, and hence is slightly older than the central crater dome.

Older flank domes

Six steep-sided mounds, ranging between 400 and 1,500 m diameter, are present on the lower island flanks (Fig. 3), with five of these located in the south-western quadrant. These features rise up to 240 m from their surrounds. The central parts of these mounds are not exposed, but based on their form and the composition of apron sediments they are assumed to be domes or exhumed cryptodomes. The poorly exposed surrounding aprons comprise massive, cemented, coarse-block-bearing breccias, with larger clasts being subrounded-rounded. Clast lithologies in-

clude gabbro, gneissic gabbro, gabbroic diorite, microgabbro and basalt, with enclaves and clasts derived from enclaves of ultramafic hornblendite. The cemented sand-grade matrix contains lithic clasts, hornblende and plagioclase crystals and stands proud of clasts in weathered exposures. The degree of weathering of these units implies a significantly greater age than that of the volcaniclastic fans emplaced around and between the mounds.

Lavas

Minor basaltic, basaltic andesite and silicic andesite lavas are locally interbedded within medial flank sequences, and are exposed usually only for 100's of metres in the upper parts of stream valleys, beneath volcaniclastic successions (Fig. 3). These are mostly well jointed, aphyric to porphyritic, hornblende- and plagioclase-bearing lavas, with at least one unit containing pyroxene and olivine. The distribution of the lavas is poorly constrained, but single flow unit volumes are estimated to be $<1\times10^7$ m^3.

Discussion

Volcanic processes during recent eruptions

In three of the major volcaniclastic associations, Dm(m) lithofacies dominates, and some units contain clasts that preserve evidence of hot emplacement (aligned clast TRM/NRM). Hot emplacement, coupled with the exclusively non-vesicular character and relatively uniform composition of the clasts, indicate that small-volume pyroclastic flows, probably block-and-ash flows (BAFs) are a dominant eruptive product on Savo. This inference is corroborated by historic accounts of glowing clouds descending the volcano flanks and kastom stories of red-hot gaseous flows. Within all sequences, interbedded Dpw(m) facies that are lithologically similar to Dm(m), are interpreted as both lahar/debris flow and BAF deposits. The reports of lahars and the presence of their deposits indicate that water was plentiful, resulting in syn-eruptive or rapid post-eruptive remobilisation of primary deposits.

Such dense-rock types of pyroclastic flow are typically derived from the gravitational collapse and mass-wasting of lava domes ("Merapi-style" BAFs; Neumann van Padang 1933; Boudon et al. 1993). Explosive dome destruction through gas overpressures ("Peléan-style" BAFs; Lacroix 1904; Robertson et al. 1998) produces deposits that contain some vesicular clasts. Dome destruction may also be followed by scoria-and-ash flows derived from collapse of Plinian or Vulcanian eruption columns ("St Vincent-style"; Anderson and Flett 1903; Miller 1994). In the absence of domes, block-and-ash or scoria-and-ash flows typically result from more open-vent gas-driven eruptions, or from collapse of dense, short-lived Vulcanian eruption columns formed via interaction of meteoric water with magma at shallow depths (e.g. Nairn and Self 1978).

The non-vesicular, highly crystalline clast lithologies in the Savo deposits suggest a degassed, shallow intrusive or dome origin. In the latter case, BAF generation may have involved Merapi-style mechanisms. Merapi-style BAFs are commonly confined to single catchments or single sectors of a cone, and occur particularly where a dome stands proud of a crater or is emplaced on the outer flanks of a volcano (Gardner et al. 1994; Ui et al 1999; Abdurachman et al. 2000). These conditions are met by the older Mbazo dome (Fig. 3), which appears the most likely source for BAF deposits in the Mbazo and Megapode Field fans. These BAF deposits were probably emplaced soon before and after the 1568 A.D. passage of the Mendaña expedition. Mendaña described constant ash cloud production from the centre of Savo, and at least one white "road" descending from the island's summit to its northern coast (Amherst and Thomson 1901), matching the location of the Mbazo and Megapode Field fans. These are the oldest of the three generations of volcaniclastic fans on the island, based on their overall drainage density and degree of incision, and appear the most likely correlative of the oldest toghavitu event. It is also possible that the Kuila fan and underlying parts of the Ndavalaka fan also formed during this eruption, correlating with the legend of how the island grew considerably during the toghavitu event.

Dm(m) units forming the upper portion of the Ndavalaka fan (Fig. 3), with an intermediate drainage density and degree of incision, appear to be BAF deposits of an eruption sometime between 1630–1670 A.D., based on the radiocarbon age of buried wood.

1830s–1840s A.D. eruptions

Dm(m) units from the 1830s–1840s eruptions appear to be concentrated within two main valleys in different sectors of the cone (Rembokola and Poghorovuraghala fans, Fig. 3), although legends suggest that most catchments of the island were affected in some way (Fig. 4b). Eyewitness accounts and legends described how, before the eruptions, the crater filled with water, and hydrothermal systems increased their activity. During the eruptions, large amounts of water were ejected in addition to dust, and rapidly repeated muffled booming noises occurred throughout the climactic phases. Both hot gas and ash flows (BAFs) and cool, watery flows (that is debris flows) were observed. Climactic phases, especially those at night, involved incandescent ejecta being thrown vertically into the air, followed by glowing avalanches descending the slopes, and widespread ash falls that affected neighbouring islands. No reports refer to persistent lava domes or any raising of the central part of the island, as might accompany dome growth.

The Rembokola and Poghorovuraghala catchments coincide with the lowest points in the present crater rim,

ca. 50 and ca. 90 m, respectively, above the top of the central crater dome, respectively. According to eyewitness reports and legends, a deep crater has existed continually on Savo. The present central crater dome has a pristine morphology and does not resemble the remnants of a much larger structure. Gravitational dome collapse may not have generated the BAFs during this latest eruption because that process would require a dome to stand proud of the crater, or be emplaced on its rim or outer flanks. The alternative is that the BAFs were produced by crater-centred blasts or collapse of crater-centred dense eruptive columns, with pyroclasts preferentially channelled into the lowest points of the crater rim.

Based on available data, the Rembokola and Poghorovuraghala BAF deposits are the most silicic erupted from Savo (Table 1). They are homogeneous, with ≥90 vol% of pyroclasts being a uniform and highly crystalline high-SiO_2 andesite to dacite and matrices dominated by crystal fragments. These compositions are consistent with derivation from a degassed dome, or cryptodome, or other shallow intrusion body. The presence of up to 10% non-juvenile clast lithologies (hornblende gabbro, basalt, basaltic andesite, hornblendite and hydrothermally altered clasts) in the Dm(m) units suggests that explosions excavated vent and conduit wall rock in addition to the essentially solid juvenile magma.

The 1830s–1840s explosions on Savo could have been driven by the entrapment of crystallisation-derived magmatic gases beneath a dome, resulting in Peléan-type blasts (e.g., Boudier et al. 1989; Robertson et al. 1998; Voight and Elsworth 2000). Although such blasts are commonly laterally directed, the trajectory could have been controlled by the crater rim topography. Peléan-style blasts are typically single events that lead to rapid decompression and a phase during which vesicular pyroclasts are erupted. Neither of these characteristics appear to be the case on Savo. Instead, eyewitnesses reported short-lived repeated explosions, most with a strong vertical component. That all ejecta appear uniformly highly crystalline may imply shallow-level explosions that did not reach underlying, presumably more fluid, magmas.

Another possible mechanism involves building gas pressures from crystallising shallow magma, possibly augmented by interaction with water of the hydrothermal system, beneath a sealed vent, leading to shallow-level, vertical Vulcanian blasts. Repeated sealing of the vent may have been due to inward collapse of highly altered and saturated rocks of the hydrothermal system. Steam generated from external water may have also contributed to gas overpressures. A factor that may have contributed to the saturation of the upper edifice is rainfall. One of the eyewitnesses reported heavy rainfall during the events; high-intensity rainfalls are common to this area during cyclonic storms, and rainfall is high year-round (3,000–5,000 mm/year; Solomon Islands Meteorological Service 2002).

Although strongly hydrothermally altered, the Sc and Pc(c) units that are common throughout PCA sequences are interpreted as near-vent surge deposits, which may relate to either of the two explosion mechanisms suggested above. Other surge deposits in MBA and FBA were probably generated by segregation of ash-cloud surges from BAFs (e.g., Fisher 1979; Fujii and Nakada 1999).

The presence of Sp, Spw and Ppw(c) units in all facies associations is interpreted to represent significant tephra-fall, which is not typical of Merapi-style eruptions (e.g., Watanabe et al. 1999), and only significant in Peléan eruptions when subsequent Vulcanian or Plinian eruptions occur (e.g., Robertson et al. 1998). The dense non-vesicular clasts within Sp, Spw and Ppw(c) appear to reflect the highly crystalline and degassed state of the erupted magma.

The exclusively non-vesicular, crystalline nature of juvenile clasts in the Dm(m), Sp, Spw and Ppw(c) lithofacies is unusual for an interpreted explosive origin (cf. Nairn and Self 1978), and implies efficient magma degassing at shallow depths before eruptions. The Savo andesite and dacite are extremely sodic (Table 1), as is the nearby Gallego field on Guadalcanal (Hackman 1980; Stanton 1994). High Na_2O may result in lower magma viscosities at super liquidus temperatures (e.g., Mysen et al. 1982) and facilitate gas escape. Similar dense-rock BAFs have been formed by early vent-clearing explosions, for example at Galeras, where only a minor juvenile component is present in deposits (Calvache and Williams 1992). At Galeras (Stix et al. 1997) pressure rise beneath solidifying magma in the conduit, coupled with hydrothermal sealing of the upper edifice, set up conditions for explosive evacuation of the upper-vent blockage. The 1982 El Chichón eruption also generated early phase, dense-rock, proximal BAFs; in this case, repeated influx of external water led to phreatomagmatic blasts (Macías et al. 1997).

Regardless of how explosions were generated on Savo, at climactic phases, ejection of incandescent pyroclasts formed dense eruption columns that collapsed to form BAFs. In some cases, the BAFs were hot enough to form aligned clast TRM in the deposits and to char incorporated vegetation.

Proximal to distal variations

PCA sequences contain volumetrically important fall, surge, BAF and lahar deposits. MBA sequences are the most uniform, being overwhelmingly dominated by very thick BAF deposits, with minor fall and surge units. FBA sequences are the most diverse, with all of the primary deposit types present, along with laharic and fluvially reworked deposits.

Many BAFs travelled up to 3 km before entering the sea. Minimum vertical height/runout distance ratios (H/L) measured from the crater rim are between 0.09 and 0.16. These values suggest either unusually high-energy flows

(cf. Yamamoto et al. 1993) or that, more likely, the true H value is considerably greater because many BAFs may have resulted from collapsing, vertical or subvertical eruption columns.

With distance from source, a major reduction in bed thickness (from >40 m in MBA to <2 m in FBA) is the main change observed in the Dm(m). The thick Dm(m) in MBA sequences may be accretions from several closely spaced BAF events. Successive volcanic debris-flow deposits can accrete with no boundaries preserved between single units (e.g., Cronin et al. 2000a). However, this process is aided by the saturated nature of debris flows and post-depositional settling. That unweathered contacts are seen between internally homogeneous units in MBA sequences suggests each unit represents a single block-and-ash flow. The thickness changes record the transition from strongly valley-confined (MBA) to unconfined (FBA) flow conditions. Evidence of erosion in MBA sequences suggests that rapidly moving BAFs swept through these channels, removing thin fine-grained deposits along the flow axis while plastering thick deposits along channel margins. Slowing of the flows and deposition probably accompanied their spread onto FBA fans, where their capacity for erosion was greatly reduced.

Based on point counting data at most described sections, overall changes in Dm(m) texture from the crater to the coast are slight. Maximum clast size decreases between MBA and FBA, but modal clast size is similar, as are the volumetric clast content, lithology and matrix nature. NRM/TRM measurements indicate that many clasts remained above Curie Point temperatures for the full 3 km, whereas others either cooled during this time or never reached such temperatures. Sedimentary structures, where present, are limited to weak planar fabric, clast strings and both normal and reverse coarse-tail grading. These all imply laminar shear in the depositional boundary layer; deposition possibly occurred via progressive accretion from the base or lateral margins of a dense flow, such as is typical for debris flows (e.g., Major 1997). The weak planar fabric is more commonly displayed in BAF deposits in FBA sequences than MBA, probably because the latter comprise deposits plastered onto channel margins and, hence, most exposures are subparallel to depositional boundary layers rather than normal to them.

The similarity in lithology plus flow and depositional processes between the Savo BAFs and debris flows makes distinguishing the origin of the deposits difficult at many outcrops. However, charcoal within BAFs [Dm(m)] is not as finely disseminated as charcoal within debris-flow units, and the former may have uniform clast NRM/TRM and degassing pipes. In addition, Dm(m) is commonly covered by thin Sp and Spw facies, which appear to represent tephra falls composed of fines elutriated from the BAF, or co-eruptive ash clouds. Dpw(m) is interpreted as either BAF or debris-flow deposits (depending on other factors at specific sites) and most commonly occurs in FBA. FBA depositional packages separated by palaeosols commonly contain interbedded debris-flow, fluvial [Pc(c), Sc] and BAF deposits. The FBA areas are envisaged to have been temporary broad fans of anastomosing braided channels, while rainfall induced high sedimentation rates through syn- and post-eruptive collapse and channelling of Dm(m) and Dpw(m) units, and subsequent localised deposition of debris flow [Dpw(m)] and fluvial sediments [Sc, Pc(c)].

Surge beds [Sc, Pc(m)] are found within all three main lithofacies associations, although they are best represented in PCA. The units within MBA and FBA are thin, and dominantly fine-grained. Some may be distal equivalents of the PCA surge deposits and most probably relate to ash-cloud surges associated with the BAFs (e.g., Fisher 1979; Fujii and Nakada 1999). Ash cloud surges are also indicated by historical reports of hot gas and dust flows that were emitted from the main valleys (Toba 1993; Cronin et al. 2000b).

Some minor catchments on the lower volcano slopes were not directly affected by BAFs. Instead, reworking of thin marginal BAF deposits, surge deposits and tephra falls occurred through fluvial and debris-flow processes, building up the FFA (Fig. 3) mostly with Pc(c) and Sc facies.

Volcanic hazards

An interpretation of the volcanic hazards for Savo hinges on the eruption mechanism determined for the latest events and the resulting BAF generation. During the toghavitu event, at about ca. 1560–1570 A.D., the Mbazo and Megapode Field fans probably formed from BAFs generated by Merapi-style collapses of the dome located in the upper Mbazo valley, or possibly a series of domes that preceded it. However, during the latest eruptions, apparently ca. 1830–1840 A.D., the upper deposits of Rembokola and Poghorovuraghala fans were probably emplaced by BAFs generated through the explosive disruption of crater domes or from collapses of short-lived, dense, vertical eruption columns, and channelled favourably into breaches in the crater rim. Given the predominance of highly crystalline, apparently degassed magma erupted in recent events, and the presence of an extensive hydrothermal system on Savo, we would expect similar eruption processes in future, including:

1. Initial eruption phase: near-vent phreatic blasts, lahars, landslides from hydrothermally altered central areas, phreatomagmatic blasts and surges, possible dome growth.
2. Climactic phase(s): either dome-centred blasts or vent-centred explosions and dense vertical eruption columns, near-vent surges, column-collapse BAFs and associated ash-cloud surges, ballistic fallout, tephra falls and lahars.
3. Waning and post-eruptive phase: secondary lahars, secondary phreatic explosions, near-vent phreatic blasts, exogenous dome formation, landslide-induced debris flows.

Of these processes, we consider the BAFs to pose the greatest risk to life, because they impact on the coastal areas and the lower slopes where the population is concentrated, and may also generate laterally spreading ash-cloud surges. Risk due to lahars may also be high, given their rapid onset, flow and propensity to spread widely once on coastal fans. Large surges could affect the whole island, but eyewitness reports and legends mostly describe flows and gas clouds being derived from the main channels. Ballistic fallout during climactic phases of eruptions could affect large portions of the island. According to legends, falling blocks apparently killed people. Presently no inhabitants are located within 1.5 km of the crater, and most are >2 km distant.

A simple three-zone map (Fig. 11A) shows areas of relative susceptibility to ground-hugging hazards including surges, BAFs and lahars. The highest hazard zone (A) is centred on the crater, main channels and FBA fans occupied during the most recent eruptions. This also takes the present crater rim geometry into account.

The intermediate hazard zone (B) encompasses catchments less likely to be affected by ground-hugging flows, as indicated by past deposition and catchment morphology, plus interfluve areas on the middle slopes. Interfluve areas near the main catchments are still likely to be subject to ash-cloud surges associated with BAFs (e.g., Fisher 1995). In addition, all parts of zone B may be affected by ballistic fallout, ash falls, large vent-derived surges and rain-triggered lahars.

The lowest hazard zone (C) comprises areas that are well protected by topography from direct line-of-sight of the crater. These small coastal areas are in the lee of the large dome structures, particularly in the south-western sector of Savo. Depositional evidence along with historical and kastom knowledge (Cronin et al. 2000b) suggests these are the safest refuge areas on the island during eruptions, at least temporarily. These areas may still be subject to significant ballistic and tephra-fall hazards during climactic eruptive phases, and access to many of them may involve crossing through parts of zone A.

Latter (1991) prepared a first-order assessment of tephra-fall hazards from Savo, giving predicted ash falls for eruption volumes of 1 km^3 at two differing times of year, when wind conditions vary. However, Latter (1991) could find no evidence of tephra deposits on the neighbouring Russell and Florida Islands generated by large eruptions at Savo. The historical and depositional evidence we have gathered suggests that Plinian or sub-Plinian eruptions are unlikely; instead, Vulcanian-type eruptions may generate the greatest tephra falls on Savo. Hence, for hazard assessment, we have used the limits of a lower-volume scenario (0.1 km^3) proposed by Latter (1991), along with the local reports of ash fall on Guadalcanal in 1830–1840 A.D., to estimate the potential area affected by ashfall from climactic phases of activity (Fig. 11B).

Warning signals of past eruptions have included an increase in the surface expression and vigour of hydrothermal activity, die-off of vegetation around the crater area, filling of the crater depression with water and pre-event earthquakes. During the last eruption, historical records and kastom stories tell that the warning signs were recognised early enough to allow some pre-event evacuation (Cronin et al. 2000b); however, as described above, during sudden onsets of climactic activity, mass evacuations were chaotic (Grover 1958). Hence, in case of future signs of reawakening, pre-evacuation of villages in hazard zone A (Fig. 11A) should be considered a high priority.

From presently available data, we suggest that the last three major eruptions occurred in ca. 1560–1570 A.D. (as seen by Mendaña and probably recorded in the toghavitu legend), sometime between 1630–1670 A.D. (the radio-

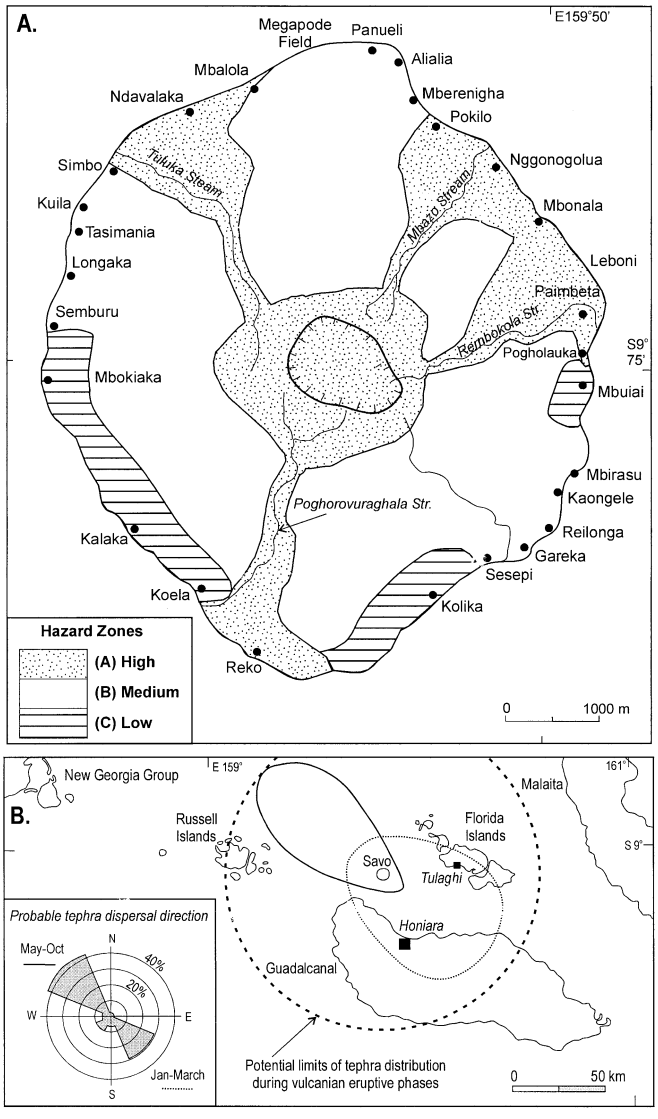

Fig. 11 Simple volcanic hazard assessment maps for Savo. **A** Flow hazards on Savo, particularly BAFs, ash-cloud surges and lahars, divided into three zones. **B** Tephra fall hazards estimated from a 0.1 km^3 eruption of Savo at two different times of the year, adapted from Latter (1991). *Inset*: wind rose diagram of surface wind directions from Hydrographer of the Navy (1988)

carbon-dated Ndavalaka fan event) and 1830–1840 A.D. (as recorded by the first Europeans in the area). These dates imply average quiescent intervals in the order of 100–200 years. Such intervals correspond with local traditional views, although other smaller events are known to have occurred in between and since, such as the lahars in 1953. Further stratigraphic and radiocarbon studies are required to establish a longer history of events.

Conclusions

The earliest of the latest three major Savo eruptions, sometime before 1568 A.D., involved the formation of a lava dome in the upper Mbazo catchment. The lava dome, which also generated block-and-ash flows, formed the large Mbazo and Megapode Field BAF deposit fans in northern Savo. Two later eruptions (1630–1670 and 1830–1840 A.D.) also produced similar BAF deposit fans, but the latter apparently involved different processes.

During the 1830s–1840s A.D. eruptions, a persistent crater-hosted vent, the absence of large domes above crater rim level, and eyewitness reports of incandescent vertical jets and subsequent glowing avalanches indicate BAF generation was via either dome-derived blasts or shallow explosions from a repeatedly sealed vent system. The highly crystalline and non-vesicular state of the juvenile pyroclasts suggests that relatively shallow explosions evacuated a degassed dome/cryptodome or conduit plug of cooled, almost solidified, magma. Common non-juvenile pyroclasts indicate incorporation of conduit wall fragments during explosive eruptions through the subvent hydrothermal system. Inward collapses of highly altered and saturated rocks of the hydrothermal system probably served to repeatedly reseal the vent.

Near-vent (<1 km) volcaniclastic sequences record fall, surge, BAF and debris-flow processes. Medial slope sequences (1 to ca. 2.5 km from vent) consist almost exclusively of thick (up to 40 m) laterally accreted deposits of valley-confined BAFs, with some ash-cloud surge and fall deposits. Large, progradational, volcaniclastic fans near the coast (2.5 to 3 km from vent) contain deposits recording all primary processes mentioned, plus fluvially reworked derivatives. These fans were probably areas of temporary, broad, anastomosing braided channels, with high local rainfall driving syn- and post-eruptive reworking of primary deposits. Transitions in BAF deposit character between these areas mostly reflect changing channel conditions, including thickness decreases from medial channel-confined to unconfined fan areas, decreases in maximum clast size and an increase in evidence of weak planar bedding structures.

Because the present Savo population of near 3,000 is located in coastal areas and upon recent volcaniclastic fans, we consider BAF, ash-cloud surge and lahar processes to pose the greatest immediate risk to life. The highest relative hazard occurs within or near the main drainage catchments whereas the lowest hazards are confined to the few coastal areas protected from direct sight of the crater by dome-cored hills. The map has been developed in consultation with local inhabitants (Cronin et al. 2000b) and is in broad agreement with their perceptions of potential refuge areas. The simple map, along with the revival of relevant traditional kastom stories, can be used to improve local awareness of volcanic hazards on Savo and encourage preparation of risk management strategies. It is also being used by government in planning development of infrastructure in the wider Savo region.

Acknowledgement The authors thank the people of Savo and officers at the Mines and Minerals Division in Honiara, without whom this paper would not have been possible. M.G.P. thanks the UK Department for International Development (UKDFID, formerly UKODA) and the British Geological Survey for their assistance and support. S.J.C. thanks the NZ Foundation for Research, Science and Technology and the Alexander von Humboldt Foundation (Germany). The authors also thank the Solomon Islands National Disaster Council, UNDHA in Suva, the Australian IDNDR Committee, and SOPAC for their encouragement and support. Drs G. Burr and D. Rex are thanked for their C^{14} and K–Ar determinations, respectively. Michel Lardy of ORSTOM and Michel Larue formerly of SOPAC are thanked for their assistance. This manuscript benefited greatly from comments by Ian Nairn, Russell Blong and Jocelyn McPhie.

References

Abdurachman EK, Bourdier JL, Voight B (2000) Nuées ardentes at Merapi Volcano, Indonesia: distribution, deposits and damage. J Volcanol Geotherm Res 100:345–361

Amherst WATA, Thomson B (1901) The discovery of the Solomon Islands by Alvaro del Mandaña in 1568; translated from the original Spanish manuscripts, vol 1. Hakluyt Society, London

Anderson T, Flett JS (1903) Report on the eruptions of the Soufière in St Vincent, in 1902 and on a visit to Montagne Peleé, In Martinique – part I. Phil Trans R Soc Lond A 200:353–553

Bascom WR (1965) Folklore and anthropology. In: Dundes A (ed) The study of folklore. Prentice-Hall, Englewood Cliffs, pp 25–33

Blong RJ (1982) The time of darkness, local legends and volcanic reality in Papua New Guinea. Australian National University Press, Canberra

Boudier JL, Boudon G, Gourgaud A (1989) Stratigraphy of the 1902 and 1929 nueé-ardente deposits, Mt Peleé, Martinique. J Volcanol Geotherm Res 38:77–96

Boudon G, Camus G, Gourgand A, Lajoie J (1993) The 1984 nuée ardente deposits of Merapi volcano, Central Java, Indonesia: stratigraphy, textural characteristics, and transport mechanisms. Bull Volcanol 55:327–342

Bronk-Ramsay C (2002) Oxcal Program v. 3.5. Oxford Radiocarbon Accelerator Unit, Oxford

Calvache MLV, Williams SN (1992) Lithic-dominated pyroclastic flows at Galeras volcano, Colombia – an unrecognised volcanic hazard. Geology 20:539–542

Cole PD, Calder ES, Druitt TH, Hoblitt R, Robertson R, Sparks RSJ, Young SR (1998) Pyroclastic flows generated by gravitational instability of the 1996–97 lava dome of Soufriere Hills volcano, Montserrat. Geophys Res Lett 25:3425–3428

Coleman PJ (1966) The Solomon Islands as an island arc. Nature 211:1249–1251

Cronin SJ, Neall VE (2000) Impacts of volcanism on Pre-European inhabitants of Taveuni, Fiji. Bull Volcanol 62:199–213

Cronin SJ, Lecointre JA, Palmer AS, Neall VE (2000a) Transformation, internal stratification and depositional processes within

a channelised, multi-peaked lahar flow. NZ J Geol Geophys 43:117–128
Cronin SJ, Petterson M. Taylor P, Planitz A (2000b) Report on the workshop on volcanic hazards, operational support planning and awareness programs for Savo Volcano, Solomon Islands. SOPAC Misc Rep 373. SOPAC, Suva, Fiji
Crook KAW, Taylor B (1994) Structural and Quaternary tectonic history of the Woodlark Triple Junction region, Solomon Islands. Mar Geophys Res 16:65–89
Fisher RV (1979) Models for pyroclastic surges and pyroclastic flows. J Volcanol Geotherm Res 6:305–318
Fisher RV (1995) Decoupling of pyroclastic currents: hazards assessments. J Volcanol Geotherm Res 66:257–263
Fujii T, Nakada S (1999) The 15 September 1991 pyroclastic flows at Unzen Volcano, Japan: a flow model for associated ash-cloud surges. J Volcanol Geotherm Res 89:159–172
Furumoto AS, Webb JP, Odegard ME, Hussong DM (1976) Seismic studies on the Ontong Java plateau 1970. Tectonophysics 34:71–90
Gardner CA, Neal CA, Waitt RB, Janda RJ (1994) Proximal pyroclastic deposits from the 1989–1990 eruption of Redoubt Volcano, Alaska – stratigraphy, distribution and physical characteristics. J Volcanol Geotherm Res 62:213–250
Grover JC (1958) Savo volcano – a potential danger to its inhabitants. In: The Solomon Islands – geological exploration and research 1953–56. Geol Surv British Solomon Islands Mem 2:108–111
Guppy HB (1887) The Solomon Islands – their geology, general features, and suitability for colonization. Swan Sonnenschein, London
Hackman BD (1980) The geology of Guadalcanal, Solomon Islands. Overseas Memoirs of the Institute of Geological Science, vol 6
Hoblitt RP, Kellog KS (1979) Emplacement temperature of unsorted and unstratified deposits of volcanic rock debris as determined by paleomagnetic techniques. Geol Soc Am Bull 90:633–642
Hydrographer of the Navy (1988) Pacific Islands pilot, vol 1, 10th edn, Solomon Islands, Papua New Guinea, Caroline Islands, Mariana Islands. Royal Australian Navy
Kroenke LW (1995) A morphotectonic interpretation of SOPAC-MAPS 1:500,000 charts. Central Solomon Islands to southern Tuvalu. SOPAC Tech Rep 220. SOPAC, Fiji
Lacroix A (1904) La montagne Peleé et ses éruptions. Masson et Cie, Paris
Latter J (1991) Volcanic hazard, risk, and risk reduction in the SW Pacific (New Zealand to Papua New Guinea). Publication of ESCAP (UN). In: Proceedings of Regional Symposium on the International Decade for Natural Disaster Reduction, Bangkok, Thailand, 11–16 February
Macías JL, Sheridan MF, Espíndola JM (1997) Reappraisal of the 1982 eruptions of El Chichón Volcano, Chiapas, Mexico: new data from proximal deposits. Bull Volcanol 58:459–471
Major J (1997) Depositional processes in large-scale debris-flow experiments. J Geol 105:345–366
Miller TP (1994) Dome growth and destruction during the 1989–1990 eruption of Redoubt volcano. J Volcanol Geotherm Res 62:197–212
Miyabuchi Y (1999) Deposits associated with the 1990–1995 eruption of Unzen volcano, Japan. J Volcanol Geotherm Res 89:139–158
Mysen BO, Virgo D, Seifert FA (1982) The structure of silicate melts: implications for chemical and physical properties of natural magma. Rev Geophys Space Phys 20:353–83
Nairn IA, Self S (1978) Explosive eruptions and pyroclastic avalanches from Ngauruhoe in February 1975. J Volcanol Geotherm Res 3:39–60
Neumann van Padang M (1933) De uitbarsting vanden Merapi (Midden Java) in de Jaren 1930–1931. Vulk Seism Meded 12:1–116
Petterson MG, Neal CR, Mahoney JJ, Kroenke L, Saunders AD, Babbs TL, Duncan R, Tolia D, McGrail B (1997) Structure and deformation of North and Central Malaita, Solomon Islands: tectonic implications for the Ontong Java Plateau–Solomon Arc collision and for the fate of ocean plateaus. Tectonophysics 283:1–33
Petterson MG, Neal CR, Mahoney, JJ, Saunders AD, Babbs T, Duncan RA, Tolia D, Magu R, Qopoto C, Mahoa H, Natogga D (1999) Geological and tectonic framework of Solomon Islands SW Pacific. Crustal accretion and growth within an intra-oceanic setting. Tectonophysics 301:35–60
Robertson R, Cole P, Sparks RSJ, Harford C, Lejeune AM, McGuire WJ, Miller AD, Murphy MD, Norton G, Stevens NF, Young SR (1998) The explosive eruption of Soufriere Hills volcano, Montserrat, West Indies, 17 September 1996. Geophys Res Lett 25:3429–3432
Solomon Islands Meterological Service (2002) Climate of Solomon Islands in brief. http://www.met.gov.sb/climate/brief.htm
Stanton RL (1994) Ore elements in arc lavas. Oxford Monogr Geol Geophys 29. Clarendon Press, Oxford
Stix J, Torres RC, Narváez, LN, Cortés GPJ, Raigosa JA, Gómez DM, Castonguay R (1997) A model of Vulcanian eruptions at Galeras volcano, Colombia. J Volcanol Geotherm Res 77:285–303
Stuiver M, Reimer PJ, Bard E, Beck JW, Burr GS, Hughen KA, Kromer B, McCormac G, van der Plicht J, Spurk M (1998) INTCAL98 radiocarbon age calibration, 24000-0 cal BP. Radiocarbon 40:1041–1083
Taylor PW (1995) Myths, legends and volcanic activity: an example from northern Tonga. J Polynesian Soc 104:323–246
Toba T (1993) Analysis of Savo custom stories on the eruption of Savo volcano. Tech Rep TR4/93, Seismol Unit, Water and Mineral Resources Division, Ministry of Energy Water and Mineral resources, Honiara, Solomon Islands
Toba T (1995) Geothermal activity of Savo volcanic island, Solomon Islands. A review and interpretation of temperature data obtained from geothermal vents during the period 1956–1993. Tech Rep TR6/95, Seismol Unit, Water and Mineral Resources Division, Ministry of Energy Water and Mineral resources, Honiara, Solomon Islands
Ui T, Matsuwo N, Sumita M, Fujinawa A (1999) Generation of block and ash flows during the 1990–1995 eruption of Unzen volcano, Japan. J Volcanol Geotherm Res 89:123–137
Voight B, Elsworth D (2000) Instability and collapse of hazardous gas-pressurised lava domes. Geophys Res Lett 27:1–4
Watanabe K, Ono K, Sakaguchi K, Takada A, Hoshizumi H (1999) Co-ignimbrite ash-fall deposits of the 1991 eruptions of Fugendake, Unzen volcano, Japan. J Volcanol Geotherm Res 89:95–112
Yamamoto T, Takarada S, Suto S (1993) Pyroclastic flows from the 1991 eruption of Unzen volcano, Japan. Bull Volcanol 55:166–175
Yan CY, Kroenke L (1993) A plate tectonic reconstruction of the Southwest Pacific, 0–100 Ma. In: Berger WH, Mayer LW (eds) 1993 Proc Ocean Drilling Prog Sci Results 130:697–709